A 3-year record of simultaneously measured aerosol chemical and optical properties at Barrow, Alaska

P. K. Quinn, T. L. Miller, and T. S. Bates
Pacific Marine Environmental Laboratory, NOAA, Seattle, Washington, USA

J. A. Ogren and E. Andrews
Climate Monitoring and Diagnostics Laboratory, NOAA, Boulder, Colorado, USA

G. E. Shaw
Geophysical Institute, University of Alaska, Fairbanks, Alaska, USA

Received 27 August 2001; revised 17 December 2001; accepted 7 January 2002; published 15 June 2002.

[1] Results are presented from 3 years of simultaneous measurements of aerosol chemical composition and light scattering and absorption at Barrow, Alaska. All results are reported at the measurement relative humidity of $\leq$40%. Reported are the annual cycles of the concentration of aerosol mass, sea salt, non-sea-salt (nss) sulfate, methanesulfonate or MSA^-, NH_4^+, and nss K^+, Mg^{+2}, and Ca^{+2} for the submicron and supermicron size ranges. Submicron nss $SO_4^=$, NH_4^+, and nss K^+, Mg^{+2}, and Ca^{+2} peak in winter and early spring corresponding to the arrival and persistence of Arctic Haze. Submicron sea salt displays a similar annual cycle presumably due to long-range transport from the northern Pacific Ocean. Supermicron sea salt peaks in summer corresponding to a decrease in sea ice extent. Submicron and supermicron MSA^- peak in the summer due to a seasonal increase in the flux of dimethylsulfide from the ocean to the atmosphere. A correlation of MSA^- and particle number concentrations suggests that summertime particle production is associated with this biogenic sulfur. Mass fractions of the dominant chemical species were calculated from the concentrations of aerosol mass and chemical species. For the submicron size range the ionic mass and associated water make up 80 to 90% of the aerosol mass from November to May. Of this ionic mass, sea salt and nss $SO_4^=$ are the dominant species. The residual mass fraction, or fraction of mass that is chemically unanalyzed, is equivalent to the ionic mass fraction in June through October. For the supermicron size range the ionic mass and associated water make up 60 to 80% of the aerosol mass throughout the year with sea salt being the dominant species. Also reported for the submicron size range are the annual cycles of aerosol light scattering and absorption at 550 nm, Ångström exponent for the 450 and 700 nm wavelength pair, and single scattering albedo at 550 nm. On the basis of linear regressions between the concentrations of sea salt and nss $SO_4^=$ and the light scattering coefficient, sea salt has a dominant role in controlling light scattering during the winter, nss $SO_4^=$ is dominant in the spring, and both components contribute to scattering in the summer. Submicron mass scattering efficiencies of the dominant aerosol chemical components (nss $SO_4^=$, sea salt, and residual mass) were calculated from a multiple linear regression of the measured light scattering versus the component concentrations. Submicron nss $SO_4^=$ mass scattering efficiencies were relatively constant throughout the year with seasonal averages ranging from 4.1 ± 2.9 to 5.8 ± 1.0 m^2 g^{-1}. Seasonal averages for submicron sea salt ranged from 1.8 ± 0.37 to 5.1 ± 0.97 m^2 g^{-1} and for the residual mass ranged from 0.21 ± 0.31 to 1.5 ± 1.0 m^2 g^{-1}. Finally, concentrations of nss $SO_4^=$ measured at Barrow were compared to those measured at Poker Flat Rocket Range, Denali National Park, and Homer for the 1997/1998 and 1998/1999 Arctic Haze seasons. Concentrations were highest at Barrow and decreased with latitude from Poker Flat to Denali to Homer revealing a north to south

0148-0227/02/2001JD001248$09.00

gradient in the extent of the haze. *INDEX TERMS:* 0305 Atmospheric Composition and Structure: Aerosols and particles (0345, 4801); 0365 Atmospheric Composition and Structure: Troposphere—composition and chemistry; 1610 Global Change: Atmosphere (0315, 0325); *KEYWORDS:* Arctic, aerosol, chemistry, optics, time series

1. Introduction

[2] The late winter-early spring maximum in aerosol light scattering, absorption, and mass concentration at Barrow is a well-documented phenomenon known as Arctic Haze. Several seasonal variations contribute to the development of Arctic Haze including stronger transport from the midlatitudes to the Arctic [e.g., *Shaw*, 1981; *Barrie et al.*, 1989; *Iversen and Joranger*, 1985] and weaker pollutant removal through wet deposition in the winter and spring [e.g., *Barrie et al.*, 1981; *Shaw*, 1981; *Heintzenberg and Larssen*, 1983]. Arctic Haze has been the subject of much study as it may change the solar radiation balance of the Arctic, affect visibility, and provide a source of contaminants to Arctic ecosystems.

[3] The goals of the National Oceanic and Atmospheric Administration's (NOAA) regional-scale aerosol monitoring program are to characterize means, variabilities, and trends of climate-forcing properties of different aerosol types and to understand the factors that control these properties. Current North American monitoring sites are located at Barrow, Alaska, Southern Great Plains, Oklahoma, and Bondville, Illinois. This paper focuses on simultaneous measurements of aerosol chemical and optical properties made at Barrow (71.32°N, 156.61°W) from October 1997 to December 2000. Seasonal changes in aerosol composition are determined along with the effect of these changes on optical properties.

[4] NOAA began aerosol observations at Barrow in 1976 using an integrating nephelometer to measure aerosol light scattering and a condensation nucleus counter to measure aerosol number concentration. In 1988 an aethalometer was added to measure light absorption by particles. Results from these measurements have been reported previously [e.g., *Polissar et al.*, 1999; *Bodhaine*, 1995; *Bodhaine and Dutton*, 1993; *Bodhaine*, 1989]. In 1997 several changes were made to the aerosol observing system. A high-sensitivity nephelometer (TSI model 3563) was installed, a continuous light absorption photometer (PSAP, Radiance Research) supplanted the aethalometer, the aerosol inlet was modified to control the relative humidity (RH) of the sampled air, and sector-controlled sampling was implemented to eliminate sampling of the locally polluted sector. In addition, routine and continuous collection of aerosol for chemical analysis (major ions and aerosol mass) was begun with an automated filter sampling system. Aerosol collected for chemical analysis is segregated into submicron and supermicron size fractions. The size segregation allows for the differentiation of aerosol that is transported over long distances (submicron size range which contains the accumulation mode) and locally generated aerosol that has a relatively short lifetime (supermicron size range which contains the coarse mode).

[5] Reported here for the first time are results from the continuous sampling of chemical and optical properties using the upgraded aerosol sampling system. This data record is the longest reported of simultaneous, year-round measurements of aerosol chemical and optical properties at Barrow. Presented are monthly mean concentrations of aerosol mass and the dominant aerosol ionic chemical components, monthly mean values of aerosol light scattering and absorption coefficients, single scattering albedo, Ångström exponent, and particle number concentration. We relate chemical and optical properties for the winter (October to January), spring (March to June), and summer (July to September) seasons through linear regressions of the light scattering coefficient against the mass concentrations of sea salt and non-sea-salt $SO_4^=$. In addition, we report mass scattering efficiencies, the parameter which directly links the mass concentration of a chemical component with its light scattering efficiency, for submicron aerosol mass, sea salt, and nss $SO_4^=$. Finally, we compare the aerosol chemical composition measured at Barrow to that measured at three more southerly sites in Alaska to determine how far south Arctic Haze extended during the 1997/1998 and 1998/1999 haze seasons. The three sites are Poker Flat Rocket Range, Denali National Park, and Homer.

[6] All measurements reported here were made at the surface. Aerosol concentrations in haze layers aloft can be much larger than surface concentrations due to the stability of the Arctic atmosphere [e.g., *Schnell et al.*, 1989]. During weaker inversions or when the inversion breaks down, aerosol may be transported vertically, and surface and aloft aerosol properties can be similar [*Bodhaine*, 1989]. During periods of a strong inversion, however, surface and aloft aerosol loadings and properties are not well correlated. Therefore it is acknowledged that measurements at the surface do not always represent the entire atmospheric column. At this time, however, continuous observations at the surface offer the most cost-effective method for identifying seasonal, annual, and longer-term trends and cycles [*Hopper et al.*, 1994].

2. Measurements at Barrow

[7] Sample air is drawn into a 21.6 cm inner diameter inlet stack at 10 m above ground level [*Delene and Ogren*, 2002]. The flow rate through the stack is approximately 1000 L min^{-1} and is divided into a sample flow of 150 L min^{-1} and a sheath flow of 850 L min^{-1}. The sample flow is taken from the center of the stack tube and drawn through a 4.45 cm inner diameter stainless steel tube where the air is heated to achieve a relative humidity of no more than 40%. The sample flow is then split into five 1.6 cm inner diameter lines each operating at a flow rate of 30 L min^{-1}. These lines feed the different aerosol instruments which are housed in a temperature-controlled building. Sampling is sector- controlled such that real-time wind speed and direction measured at the top of the inlet are used to exclude data from the locally polluted sector (130° to 360°).

[8] Sample relative humidity (RH) is measured after the heater and directly upstream of the aerosol instruments. The amount of heating required to maintain this low reference

RH varies with season. From 1997 through 2000, heating averaged 31° ± 8°C in spring, 14° ± 3°C in summer, 25° ± 8°C in fall, and 38° ± 7°C in winter to maintain a sample RH between 20 and 40%. The aerosol is heated to maintain a relatively stable reference RH that allows for constant instrumental size segregation in spite of variations in ambient RH. Chemical, physical, and optical measurements are all made at this reference RH and thus are all directly comparable. In addition, measurement at a low reference RH makes it possible, with the knowledge of appropriate growth factors, for end users of the data set (process, chemical transport, and radiative transfer models) to adjust the measured parameters to a desired relative humidity. All measurements are reported at the reference RH.

[9] The sample air for determination of aerosol chemical composition and mass concentration first enters a Berner-type multijet cascade impactor [*Berner et al.*, 1979] with aerodynamic D_{50} cutoff diameters of 10 and 1 μm. A 12 μm grease cup is coated with silicone grease, and a film coated with silicone spray is placed on the 10 μm jet place to minimize bounce of large particles onto the downstream stages. Particles with aerodynamic diameters between 1 and 10 μm are collected on a Tedlar film. Particles with diameters less than 1 μm pass through the impactor to a filter carousel housing 8 Millipore Fluoropore filters (1.0 μm pore size). Computer-controlled solenoid valves downstream of the filters open and close sequentially so that one filter is sampled at a time. Submicron filter samples are collected over a period of 1 to 5 days depending on the time of year and the aerosol loading. One filter serves as a sampling blank and is exposed to sample air for 10 s. One supermicron sample is collected with the impactor during the time it takes to sample all of the submicron filters in the carousel. All handling of the impactor films and carousel filters is done in a glove box purged with air that has passed through a scrubber containing potassium carbonate and citric acid to remove SO_2 and NH_3. After collection, samples are shipped to NOAA's Pacific Marine Environmental Laboratory (PMEL) for analysis in sealed tubes.

[10] At PMEL the films and filters are wetted with 1 mL of spectral grade methanol. An additional 5 mL of distilled deionized water are added to the solution, and the substrates are extracted by sonicating for 30 min. Concentrations of major cations (Na^+, NH_4^+, K^+, Mg^{2+}, Ca^{2+}) and anions (methanesulfonate or MSA^-, Cl^-, NO_3^-, $SO_4^=$) are determined by ion chromatography [*Quinn et al.*, 1998]. All handling of substrates is done in a glove box similar to that at Barrow. NO_3^- concentrations are not reported because of the uncertainties associated with heating of the aerosol to maintain a sample RH below 40%. Heating by the amounts required (an average of 14°C in summer to 38°C in winter) may lead to substantial volatilization of ammonium nitrate from the substrate resulting in artificially low nitrate concentrations [*Meyer et al.*, 1992; *Ayers et al.*, 1999].

[11] Non-sea-salt sulfate (nss $SO_4^=$) concentrations are initially calculated from Na^+ concentrations and the mass ratio of sulfate to sodium in seawater of 0.252 [*Holland*, 1978]. Negative nss $SO_4^=$ concentrations resulting from this approach have been reported for Antarctic winter aerosol [e.g., *Wagenbach et al.*, 1988, 1998] and have been attributed to depletion of sea salt $SO_4^=$ through fractionation processes. On the basis of sulfur isotope analysis, sea salt $SO_4^=$ depletion also has been reported for the Canadian Arctic [*Norman et al.*, 1999]. Calculation of nss $SO_4^=$ for the submicron size range using the $SO_4^=$ to Na^+ seawater mass ratio of 0.252 did not yield negative values. Therefore this approach was used for the submicron size range. Negative nss $SO_4^=$ concentrations did result for the supermicron size range, however. As per the method of *Wagenbach et al.* [1998], supermicron nss $SO_4^=$ concentrations were calculated by performing a linear regression of nss $SO_4^=$ calculated using the 0.252 mass ratio versus Na^+ for the winter, spring, and summer seasons. The obtained negative slope was then added to the conventional ratio of 0.252. Resulting supermicron $SO_4^=$ to Na^+ seawater mass ratios were 0.13 for winter (October to February), 0.082 for spring (March to June), and 0.23 for summer (July to September).

Table 1. Distributions of Trajectories as Percentages Arriving at Barrow From Six Different Source Regions for the Winter (October to January), Spring (March to June), and Summer (July to September) Seasons[a]

Source Region	October–January	March–June	July–September
East Arctic Basin	27	18	17
North America	16	17	13
Pacific	7.8	23	22
Russia	5.2	2.5	1.4
Siberia	18	14	15
West Arctic Basin	27	25	31

[a] The back trajectories were calculated twice daily for an arrival height of 500 m.

[12] For the comparison of Barrow and Alert nss $SO_4^=$ seasonal cycles, the submicron and supermicron Barrow concentrations were summed for a more direct comparison to the high-volume, non-size-segregated Alert samples. (Seven day aerosol samples were collected at Alert on 20 cm by 25 cm Whatman 41 filters using a high-volume sampler [*Sirois and Barrie*, 1999]. The face velocity of sampling (50 cm s^{-1}) and typical filter loadings ensured collection efficiencies better than 95% [*Watts et al.*, 1987]). Alert nss $SO_4^=$ concentrations were calculated using the 0.252 $SO_4^=$ to Na^+ mass ratio since this did not yield any negative nss $SO_4^=$ concentrations.

[13] Sea salt aerosol concentrations are calculated as

$$\text{sea salt}\left(\mu g\, m^{-3}\right) = Cl^-\left(\mu g\, m^{-3}\right) + Na^+\left(\mu g\, m^{-3}\right) \times 1.47, \quad (1)$$

where 1.47 is the seawater ratio of ($Na^+ + K^+ + Mg^{+2} + Ca^{+2} + SO_4^= + HCO_3^-$)/$Na^+$ [*Holland*, 1978]. Cl^- in excess of the Cl^- to Na^+ seawater ratio of 1.8 was not added to the sea salt mass. This approach prevents the inclusion of nss K^+, Mg^{+2+}, Ca^{+2}, $SO_4^=$, and HCO_3^- in the sea salt mass and allows for the loss of Cl^- mass through Cl^- depletion processes. It also assumes that all Na^+ is derived from seawater. Results of *Barrie and Barrie* [1990] indicate that the majority of Na^+ in the Arctic is associated with sea salt that is either unmodified or anthropogenically modified.

[14] All ion concentrations are reported at 0°C and 1013 mbar. Throughout the paper, submicron refers to particles with aerodynamic diameters (D_{aero}) less than 1 μm, and supermicron refers to particles with aerodynamic diameters

Table 2. Submicron Mass Concentrations at Barrow, Alaska, for October 1997 to December 2000[a]

	μg m^{-3}								
	Mass[b]	Sea Salt[c]	nss $SO_4^{=}$[d]	NH_4^{+}[e]	MSA^{-}[f]	nss K^{+}[g]	nss Mg^{+2}[h]	nss Ca^{+2}[i]	Residual[j]
Jan.	3.8 ± 2.2	1.1 ± 1.1	0.78 ± 0.43	0.23 ± 0.09	<0.0001	0.03 ± 0.03	0.09 ± 0.11	0.03 ± 0.03	0.62 ± 1.0
Feb.	3.5 ± 1.7	0.93 ± 1.1	0.91 ± 0.39	0.26 ± 0.09	<0.0001	0.03 ± 0.02	0.06 ± 0.07	0.02 ± 0.03	0.56 ± 0.57
March	2.6 ± 1.3	0.68 ± 0.73	0.71 ± 0.44	0.21 ± 0.12	<0.0001	0.02 ± 0.01	0.03 ± 0.04	0.01 ± 0.01	0.41 ± 0.69
April	2.1 ± 1.1	0.43 ± 0.61	0.72 ± 0.36	0.19 ± 0.07	0.002 ± 0.002	0.01 ± 0.01	0.008 ± 0.01	0.003 ± 0.005	0.32 ± 0.40
May	1.2 ± 0.60	0.15 ± 0.15	0.60 ± 0.50	0.14 ± 0.06	0.01 ± 0.01	0.005 ± 0.004	0.002 ± 0.003	0.006 ± 0.009	0.08 ± 0.10
June	0.89 ± 1.1	0.05 ± 0.10	0.19 ± 0.21	0.06 ± 0.05	0.01 ± 0.02	0.002 ± 0.002	0.0003 ± 0.0006	0.004 ± 0.008	0.45 ± 1.1
July	0.60 ± 0.49	0.08 ± 0.09	0.10 ± 0.10	0.03 ± 0.03	0.01 ± 0.01	0.001 ± 0.001	<0.0001	0.005 ± 0.01	0.27 ± 0.25
Aug.	0.81 ± 0.82	0.17 ± 0.22	0.08 ± 0.06	0.02 ± 0.01	0.01 ± 0.01	0.001 ± 0.001	<0.0001	0.001 ± 0.002	0.40 ± 0.33
Sept.	0.61 ± 0.44	0.17 ± 0.11	0.09 ± 0.12	0.02 ± 0.04	0.007 ± 0.004	0.001 ± 0.001	<0.0001	0.002 ± 0.005	0.26 ± 0.37
Oct.	2.0 ± 1.6	0.74 ± 0.98	0.13 ± 0.16	0.05 ± 0.06	0.0009 ± 0.001	0.002 ± 0.007	0.0003 ± 0.001	0.02 ± 0.07	0.93 ± 1.2
Nov.	1.4 ± 1.2	0.62 ± 0.86	0.13 ± 0.09	0.05 ± 0.04	0.0002 ± 0.0005	0.003 ± 0.006	0.001 ± 0.003	0.009 ± 0.02	0.30 ± 0.45
Dec.	3.1 ± 3.0	1.1 ± 1.2	0.32 ± 0.23	0.09 ± 0.05	0.0001 ± 0.0003	0.01 ± 0.01	0.02 ± 0.02	0.009 ± 0.01	0.55 ± 0.44

[a] Concentrations are reported as arithmetic mean and standard deviation (1σ) at 0°C and 1013 mbar.
[b] Uncertainties for low and high concentrations of mass are 0.6 ± 5.5% and 3.0 ± 5.2% μg m^{-3} (concentration ± 95% uncertainty).
[c] Uncertainties for low and high concentrations of sea salt are 0.2 ± 9.6% and 1.0 ± 6.1% μg m^{-3} (concentration ± 95% uncertainty).
[d] Uncertainties for low and high concentrations of nss $SO_4^{=}$ are 0.05 ± 7.0% and 1.0 ± 6.0% μg m^{-3} (concentration ± 95% uncertainty).
[e] Uncertainties for low and high concentrations of NH_4^{+} are 0.01 ± 39% and 0.2 ± 7.8% μg m^{-3} (concentration ± 95% uncertainty).
[f] Uncertainties for low and high concentrations of MSA^{-} are 0.0005 ± 6.0% and 0.01 ± 6.0% μg m^{-3} (concentration ± 95% uncertainty).
[g] Uncertainties for low and high concentrations of nss K^{+} are 0.001 ± 14% and 0.03 ± 6.1% μg m^{-3} (concentration ± 95% uncertainty).
[h] Uncertainties for low and high concentrations of nss Mg^{+2} are 0.0005 ± 16% and 0.09 ± 6.2% μg m^{-3} (concentration ± 95% uncertainty).
[i] Uncertainties for low and high concentrations of nss Ca^{+2} are 0.004 ± 69% and 0.03 ± 48% μg m^{-3} (concentration ± 95% uncertainty).
[j] Calculated from the gravimetric mass less the ionic mass and associated water. Uncertainties for low and high concentrations of residual mass are 0.3 ± 51% and 1.0 ± 21% μg m^{-3} (concentration ± 95% uncertainty). Uncertainties for low and high concentrations of H_2O are 0.11 ± 33% and 3.0 ± 5.3% μg m^{-3} (concentration ± 95% uncertainty) at 33% RH.

$1.0 < D_{aero} < 10$ μm at the sample RH of ≤40%. Uncertainties at the 95% confidence level for a typical low and high concentration for each ionic species are given in Table 2. Uncertainties in the ionic species include errors due to the ion chromatography analysis, blank levels, the volume of the liquid extract, and the volume of the air sampled. All uncertainties shown in Table 2 were propagated as a quadratic sum of all errors involved which assumes that all errors were random. Details of the uncertainty analysis are given by *Quinn et al.* [2000].

[15] Submicron aerosol mass concentrations are determined by weighing the Millipore filters at PMEL before and after sample collection with a Mettler UMT2 microbalance [*Quinn et al.*, 2000]. Supermicron aerosol mass concentrations are determined by weighing the Tedlar films with a Cahn Model 29 microbalance. Both microbalances are housed in a glove box kept at 33 ± 3% RH. Maintaining the glove box at a constant RH allows each sampled substrate to come into equilibrium with the same vapor pressure of water, thus reducing experimental uncertainty due to variable laboratory RH. The reported mass concentrations include the water mass that is associated with the aerosol on the filter at the glove box RH. All aerosol mass concentrations are reported at 0°C, 1013 mbar, and the sample RH. Uncertainties at the 95% confidence level for a typical low and high mass concentration are given in Table 2. Uncertainties in the aerosol mass include errors due to weighing, blank levels, storage and transport, and the volume of air sampled [*Quinn et al.*, 2000].

[16] Residual mass concentrations, or the mass of the chemically unanalyzed species, were calculated from the gravimetrically determined aerosol mass less the mass of the ionic species and water. Uncertainties at the 95% confidence level for a typical high and low residual mass concentration are given in Table 2. Uncertainties in the residual mass include errors due to the concentrations of the ionic species, the aerosol mass, and water [*Quinn et al.*, 2000].

[17] Measurements of aerosol scattering coefficients were made at wavelengths of 450, 550, and 700 nm at an RH between 20 and 40% with a TSI 3563 nephelometer [*Delene and Ogren*, 2002]. Two Berner-type impactors are operated upstream of the nephelometer. The sample airflow is switched every 5 min between the two impactors so that scattering by either submicron or sub-10 μm particles is measured. Values measured directly by the nephelometer are corrected as per *Anderson and Ogren* [1998] for an offset determined by measuring filtered air and for angular nonidealities of the nephelometer including truncation errors and nonlambertian response. Values are reported at 0°C, 1013 mbar, and the sample RH.

[18] The uncertainty associated with the scattering measurements include errors due to noise, calibration, angular nonidealities, and adjustment to STP. Using the method of *Anderson and Ogren* [1998], the overall uncertainty of the light scattering coefficient at 550 nm was estimated to be 7.8% for a 24-hour averaging time.

[19] Aerosol absorption coefficients are measured by monitoring the change in transmission through a filter with a Particle Soot Absorption Photometer (PSAP, Radiance Research). The PSAP is located downstream of the impactors to determine both submicron and sub-10 μm absorption coefficients. Measured values are corrected for a scattering artifact, the deposit spot size, the PSAP flow rate, and the manufacturer's calibration as per *Bond et al.* [1999]. Values are reported at 550 nm, 0°C, 1013 mbar, and the sample RH. The uncertainty associated with the absorption measurements include errors due to calibration, noise, and adjustment to STP and 550 nm. Using the method of *Bond et al.* [1999], the overall uncertainty of the absorption coefficient at 550 nm was estimated to be 22% for a 24-hour averaging time. Scattering and absorption coefficients were averaged over the period of the submicron filter samples and include only times when sample air was drawn through the filters.

[20] Aerosol number concentration is measured with a TSI model 3760 condensation particle counter. The reported number concentration includes all particles with diameters greater than 14 nm at the sample RH. Number concentrations were averaged over the period of the daily submicron filter samples and include only times when sample air was drawn through the filters.

[21] Air mass back trajectories were calculated for three arrival heights (500, 2500, and 5500 m) for the station location at 12-hour intervals. Trajectories were calculated with the Hybrid Single-Particle Lagrangian Integrated Trajectory (HY-SPLIT 4) model based on the FNL global wind field [*Draxler*, 1992].

[22] The gravimetric analysis was performed at 33% RH. Hence the measured mass on the sampling substrates included the amount of water associated with the aerosol at that RH. The chemical thermodynamic equilibrium model AeRho [*Quinn et al.*, 1998] was used to estimate the water mass associated with the inorganic ions at 33% RH so that mass fractions of the aerosol chemical components could be calculated from the gravimetric and ionic mass. Uncertainties at the 95% confidence level are reported for a typical low and high H_2O concentration in Table 2. Uncertainties in the water calculation include errors due to the measured chemical composition, the glove box RH and temperature, and the volume of air sampled. See *Quinn et al.* [2000] for details of the uncertainty calculations.

[23] AeRho is a static model. It is designed to take the measured ionic composition of the aerosol and the constant sampling RH and to determine the molecular composition of the ionic chemical species within the aerosol. The molecular composition then is used to calculate the water mass associated with the aerosol species. The model is not used to describe a dynamic system in which changes in the concentration of gas phase species affect the aerosol molecular composition. Therefore it does not include interactions between the gas and aqueous phases. In addition, because of the constant sampling RH, it is not necessary to take into account changes in particle size with changes in RH. More details about the model are given by *Quinn et al.* [1998] and *Quinn and Coffman* [1998].

3. Results: Trajectory Analysis

[24] As pointed out by *Lowenthal and Rahn* [1985], the use of trajectories to reconstruct the history of sampled air masses in the Arctic is difficult because of the large distances to the source regions (5000 to 10,000 km or 5 to 20 days transit time) and sparse meteorological data. Knowing the limits of Arctic trajectory analysis, twice daily back trajectories were calculated to determine if a seasonal pattern existed in source regions to Barrow during the October 1997 to December 2000 measurement period. Trajectories calculated 7 days back in time and arriving at a height of 500 m were initially grouped into eight source regions including the East Arctic Basin (0° to 180°E and north of contiguous landmasses), West Arctic Basin (0° to 180°W and north of contiguous landmasses), North America, the Pacific Ocean, Russia (30°E to 90°E), Siberia (90°E to eastern edge of Russia), Europe, and the Atlantic Ocean. Because of the scarcity of trajectories from Europe and the Atlantic, the number of source regions was reduced to six.

[25] Table 1 shows the distributions of the source regions for winter (October to January), spring (March to June), and summer (July to September). The data were segregated based on similarities in the submicron nss $SO_4^=$ and sea salt concentrations for these time periods. February was not included as it appeared to be a transitional month between the winter and spring seasons. The large frequency of trajectories from the East and West Arctic Basins indicates that 7 day back trajectories often do not allow for the determination of the source region. Unfortunately, accuracy of the trajectory analysis decreases with each day back in time. Seasonal differences are not large, but it is apparent that winter has the fewest trajectories from North America and the Pacific and the most from the East Arctic Basin, Russia, and Siberia. On the basis of trace elemental analysis, midlatitude regions in Russia and Siberia have been identified as significant sources of pollutant aerosol to the Arctic [*Rahn*, 1981a, 1981b; *Lowenthal and Rahn*, 1985]. Distributions of source regions for spring and summer are not significantly different. Of those trajectories traveling back to Russia and Siberia, a higher percentage traveled more than 4000 km during the winter (50%) than during the spring (30%) or summer (20%). This analysis suggests that Arctic Haze results from winter and spring episodic injections of pollutant aerosols from the midlatitudes to the Arctic. These aerosols then pool in the Arctic Basin since removal by wet deposition is slow during this time of year. These results are in agreement with those previously published [e.g., *Bridgman and Bodhaine*, 1994; *Barrie et al.*, 1981].

4. Results: Chemical Composition

4.1. Mass Fractions of Ionic Components

[26] Since the chemical analysis included only ionic species, measurements of the concentrations of these species and the total aerosol mass were used to determine what fraction of the aerosol mass was being taken into account. Mass fractions of the submicron and supermicron ionic chemical components were calculated as the mass concentration of the component divided by the gravimetric mass. Shown in Figures 1 and 2 are percentile information for the submicron and supermicron mass fractions of the ionic mass (including associated water at 33% RH), sea salt, nss $SO_4^=$, H_2O calculated by AeRho to be associated with the ionic species at 33% RH, and the residual mass. The residual mass is defined as the gravimetric mass less the mass of the ionic components and associated water. Sea salt, nss $SO_4^=$, and the residual component dominate the aerosol mass. The remaining ionic species (MSA^-, nss K^+, nss Mg^{+2}, and nss Ca^{+2}), although useful tracers of the source of the aerosol, contribute less than 10 and 4% to the aerosol submicron and supermicron mass, respectively. NH_4^+ contributes, on average, 6.5 ± 4.4% (arithmetic mean and 1σ standard deviation), 11 ± 4.3%, and 4.2 ± 2.9% to the submicron mass during the winter (October to January), spring (March to June), and summer (July to September), respectively. NH_4^+ contributes, on average, less than 1% to the supermicron mass.

[27] The ionic mass and associated water make up 80 to 100% of the submicron aerosol mass during the months of November to May (Figure 1). Of this ionic mass, sea salt

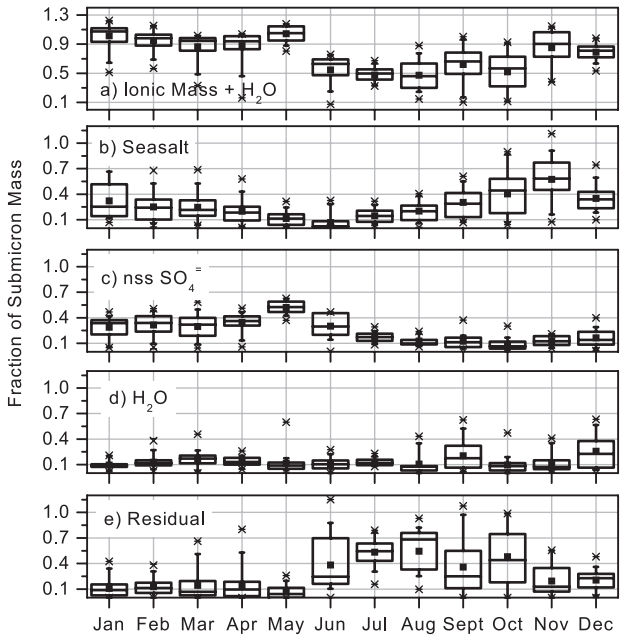

Figure 1. Box plots of submicron mass fractions of (a) ionic mass (includes sea salt, nss $SO_4^=$, nss K^+, nss Mg^{+2}, nss Ca^{+2}, NH_4^+, MSA^-, Cl^- not associated with sea salt, NO_3^-, and water associated with the ionic components at 33% RH), (b) sea salt, (c) nss $SO_4^=$, (d) water associated with the ionic components at 33% RH, and (e) residual mass (calculated as gravimetric mass less the mass of ionic species and associated water). The horizontal lines in the box denote the 25th, 50th, and 75th percentile values. The error bars denote the 5th and 95th percentile values. The two symbols below the 5th percentile error bar denote the 0th and 1st percentile values, and the two symbols above the 95th percentile error bar denote the 99th and 100th percentiles. The square symbol in the box denotes the arithmetic mean.

and nss $SO_4^=$ are the dominant species. The sea salt mass fraction is larger than that of nss $SO_4^=$ during the winter months (October to January). Sea salt and nss $SO_4^=$ mass fractions are comparable in February and March, and the nss $SO_4^=$ mass fraction is larger in April through June. The residual mass fraction is less than 20% during November to May but becomes comparable to the ionic mass fraction in June through October. Particulate organic matter most likely is a large component of the residual mass. *Li and Winchester* [1989] measured the aerosol chemical composition at Barrow from March to May 1986 and found that contributions of organic acid anions (formate, acetate, propionate, and pyruvate) and inorganic anions to the aerosol mass were comparable. The higher residual mass fractions measured during the summer most likely are of biogenic origin since there is no strong source of anthropogenic aerosol during this time of year.

[28] On the basis of monthly averages the ionic mass and associated water make up 60 to 80% of the supermicron aerosol mass throughout the year (Figure 2). Of the ionic mass, sea salt is the dominant species, contributing 60 to 98% on a monthly basis. The largest contribution (>90%) of sea salt to the ionic mass occurs between July and December. Non-sea-salt $SO_4^=$ makes a relatively small contribution to the supermicron aerosol mass. It contributes, on a monthly basis, less than 1 to 16% with the largest contributions in the late winter/early spring months. The mass fraction of residual mass is fairly constant throughout the year with monthly averages ranging from 20 to 39%. Again, based on the results of *Li and Winchester* [1989], organic species most likely comprise a large portion of this residual mass.

4.2. Seasonal Cycles of the Dominant Ionic Chemical Components

[29] Sea salt aerosol results from the wind-driven production and subsequent evaporation of sea spray. Submicron sea salt concentrations increase in October, peak in December and January, begin a steady decrease in February, and reach lowest concentrations in the summer months of May through September (Figure 3b). During the peak months of December and January, mean submicron concentrations equal 1.1 ± 1.1 $\mu g\ m^{-3}$ (arithmetic mean and 1σ standard deviation) (Table 2). Supermicron sea salt concentrations display a very different seasonal cycle with concentrations increasing in July, peaking in August to October, and decreasing in November and December (Figure 4b). Lowest concentrations are observed in January through June. During the peak months the arithmetic mean of the

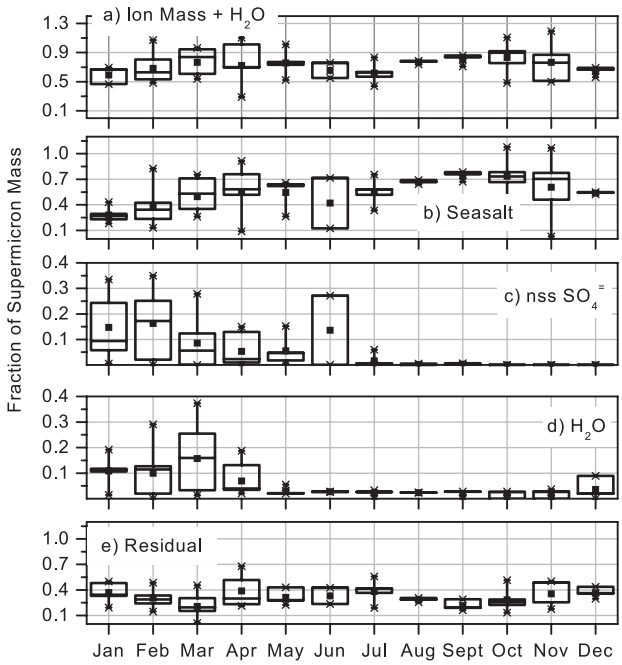

Figure 2. Box plots of supermicron mass fractions of (a) ionic mass (includes sea salt, nss $SO_4^=$, nss K^+, nss Mg^{+2}, nss Ca^{+2}, NH_4^+, MSA^-, Cl^- not associated with sea salt, NO_3^-, and water associated with the ionic components at 33% RH), (b) sea salt, (c) nss $SO_4^=$, (d) water associated with the ionic components at 33% RH, and (e) residual mass (calculated as gravimetric mass less the mass of ionic species and associated water). Percentile information is as in the Figure 1 caption.

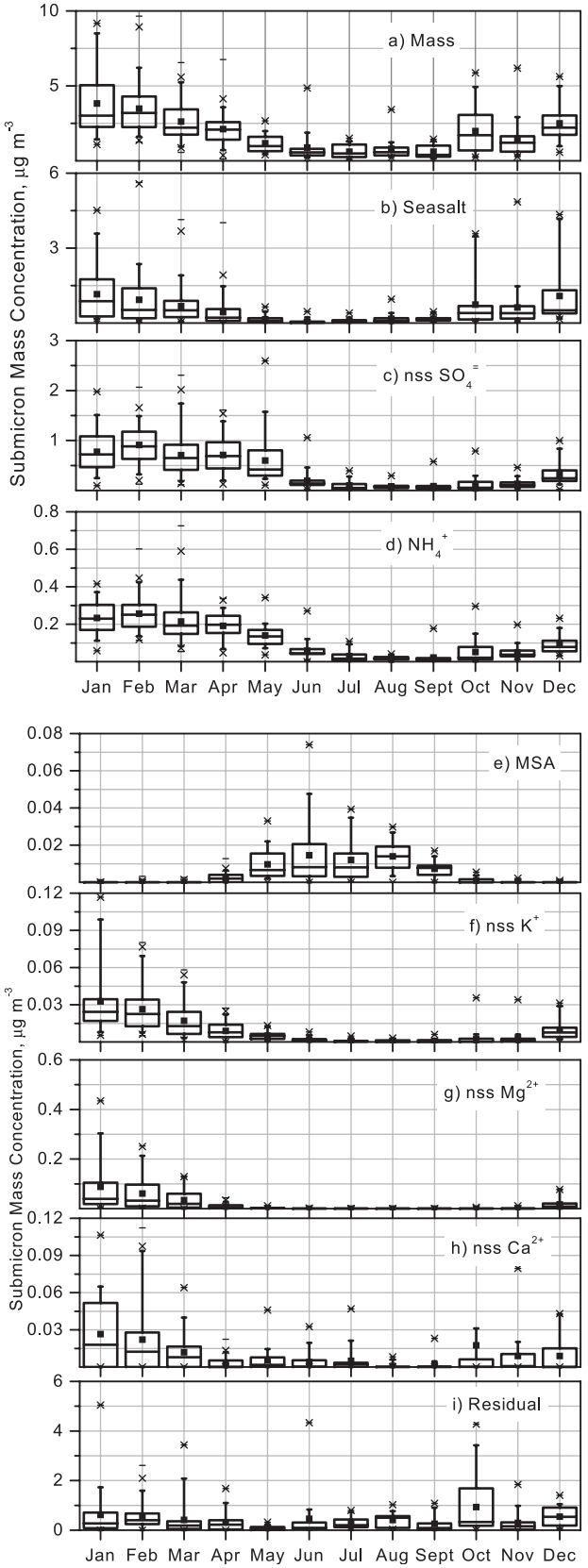

Figure 3. Box plots of submicron concentrations of (a) gravimetrically determined aerosol mass, (b) sea salt, (c) nss $SO_4^=$, (d) NH_4^+, (e) MSA^-, (f) nss K^+, (g) nss Mg^{+2}, (h) nss Ca^{+2}, and (i) residual mass as a function of month. Percentile information is as in the Figure 1 caption.

supermicron concentration ranges from 1.4 to 2.1 μg m^{-3} (Table 3).

[30] The winter maximum in Arctic submicron sea salt concentrations has been attributed to seasonally high winds in high-latitude source regions of the Pacific and Atlantic Oceans and long-range transport to the Arctic [*Sturges and Barrie*, 1988; *Sirois and Barrie*, 1999; *Quinn et al.*, 2000]. Maximum supermicron sea salt concentrations at Barrow occur during the summer when the ice pack extent is at a minimum. In addition, long-range south-to-north transport is weaker during the summer months, and aerosol removal by wet deposition is stronger. Hence the summer maximum in supermicron sea salt appears to result from local open leads and oceanic waters.

[31] Alert, located in the Canadian Arctic on the northern tip of Ellesmere Island (82.5°N, 62.3°W) is another station with a long-term record of aerosol chemistry. The 15-year data record covering 1980 to 1995 has been described by *Sirois and Barrie* [1999]. A comparison of annual cycles of sea salt, nss $SO_4^=$, and MSA from Barrow and Alert is shown in Figure 5. Submicron and supermicron concentrations from Barrow were summed for a more direct comparison to the Alert data that were derived from a high-volume sampler with no size segregation. A winter maximum in sea salt is observed at Alert such that mean concentrations are highest in November through February. Concentrations decrease in March and April and are at a minimum in May through September. The arithmetic mean concentrations during the winter maximum at Alert are a factor of 2 to 3 lower than those measured at Barrow, most likely due to the longer distance from oceanic source

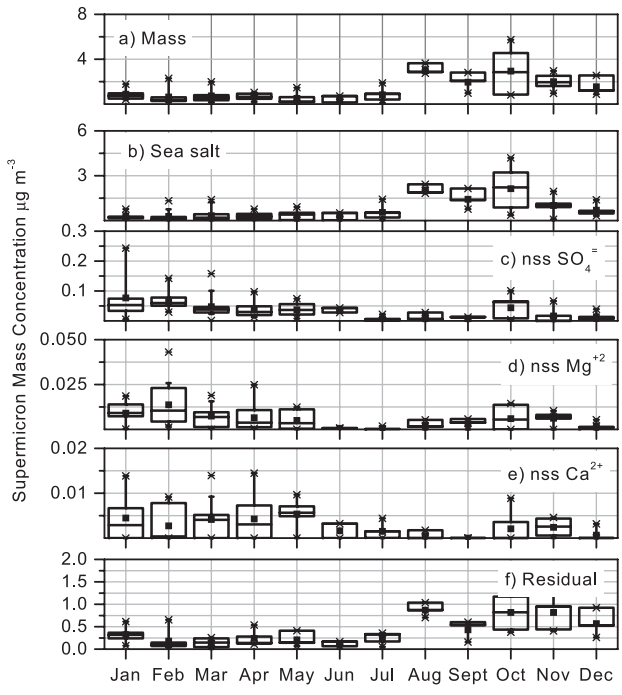

Figure 4. Box plots of supermicron concentrations of (a) gravimetrically determined aerosol mass, (b) sea salt, (c) nss $SO_4^=$, (d) nss Mg^{+2}, (e) nss Ca^{+2}, and (f) residual mass as a function of month. Percentile information is as in the Figure 1 caption.

Table 3. Supermicron Mass Concentrations at Barrow, Alaska, for October 1997 to December 2000[a]

	μg m^{-3}							
	Mass	Sea Salt	nss $SO_4^=$	NH_4^+	MSA^-	nss Mg^{+2}	nss Ca^{+2}	Residual[b]
Jan.	0.87 ± 0.55	0.32 ± 0.28	0.08 ± 0.08	0.006 ± 0.003	<0.0001	0.009 ± 0.007	0.004 ± 0.006	0.32 ± 0.19
Feb.	0.63 ± 0.67	0.28 ± 0.39	0.06 ± 0.03	0.007 ± 0.004	<0.0001	0.01 ± 0.01	0.003 ± 0.004	0.18 ± 0.20
March	0.72 ± 0.60	0.33 ± 0.44	0.05 ± 0.04	0.006 ± 0.005	<0.0001	0.007 ± 0.006	0.004 ± 0.004	0.13 ± 0.10
April	0.64 ± 0.31	0.29 ± 0.23	0.04 ± 0.03	0.004 ± 0.004	0.0001 ± 0.0002	0.006 ± 0.007	0.004 ± 0.005	0.24 ± 0.18
May	0.51 ± 0.58	0.34 ± 0.35	0.04 ± 0.02	0.003 ± 0.005	0.0004 ± 0.0005	0.005 ± 0.005	0.005 ± 0.003	0.21 ± 0.18
June	0.43 ± 0.39	0.26 ± 0.35	0.04 ± 0.01	0.003 ± 0.004	0.0007 ± 0.0007	0.001 ± 0.0004	0.002 ± 0.002	0.11 ± 0.07
July	0.82 ± 0.78	0.55 ± 0.62	0.01 ± 0.01	0.0004 ± 0.0005	0.0005 ± 0.0005	0.0005 ± 0.001	0.001 ± 0.002	0.23 ± 0.14
Aug.	3.1 ± 0.49	2.0 ± 0.33	0.01 ± 0.01	0.002 ± 0.002	0.001 ± 0.001	0.002 ± 0.003	0.001 ± 0.001	0.87 ± 0.17
Sept.	1.9 ± 0.92	1.4 ± 0.69	0.01 ± 0.01	0.0005 ± 0.0005	0.0008 ± 0.0008	0.003 ± 0.003	<0.0001	0.43 ± 0.24
Oct.	2.9 ± 1.9	2.1 ± 1.4	0.04 ± 0.04	0.0006 ± 0.001	<0.0001	0.006 ± 0.007	0.002 ± 0.004	0.82 ± 0.41
Nov.	2.0 ± 0.78	1.0 ± 0.67	0.02 ± 0.03	0.0006 ± 0.001	<0.0001	0.006 ± 0.004	0.002 ± 0.002	0.82 ± 0.50
Dec.	1.5 ± 0.89	0.69 ± 0.41	0.01 ± 0.01	0.002 ± 0.003	<0.0001	0.002 ± 0.002	0.001 ± 0.001	0.57 ± 0.33

[a] Concentrations are reported as arithmetic mean and standard deviation (1σ) at 0°C and 1013 mbar.
[b] Calculated from the gravimetric mass less the ionic mass and associated water.

regions. With no summer maximum, the Alert sea salt mean concentrations are a factor of 10 to 18 lower than those measured at Barrow.

[32] Non-sea-salt $SO_4^=$ in the Arctic has several sources [*Ferek et al.*, 1995; *Li et al.*, 1993; *Barrie et al.*, 1981]. Marine biogenic nss $SO_4^=$ is derived from the oxidation of atmospheric dimethylsulfide (DMS) which, in turn, results from oceanic phytoplankton processes. Anthropogenic sources include the burning of fossil fuels and smelting of sulfide ores in Eurasia.

[33] Submicron nss $SO_4^=$ concentrations at Barrow begin to increase in December and have a broad peak from January to May (Figure 3c and Table 2). They drop off sharply in June and remain low through November. Several factors may contribute to the broad January to May peak including the long-range transport of anthropogenic primary nss $SO_4^=$, the long-range transport of anthropogenic SO_2 that is then photooxidized to nss $SO_4^=$, and local production of biogenic nss $SO_4^=$ from the oxidation of DMS. *Barrie and Hoff* [1984] attributed the March to April peak in nss $SO_4^=$ observed in the Canadian Arctic to the enhanced photooxidation of SO_2 to nss $SO_4^=$ as light levels increase. *Ferek et al.* [1995] reported the presence of DMS in Arctic waters under the ice as early as April and suggested that as the ice recedes this DMS may be converted to nss $SO_4^=$ and contribute to late spring concentrations. Elevated nss $SO_4^=$ concentrations in May coincide with an increase in MSA concentrations (Figure 3e), a species of pure biogenic origin. Hence a biogenic source may contribute to the elevated nss $SO_4^=$ concentrations observed in May.

[34] A linear regression of nss $SO_4^=$ concentrations versus the aerosol light absorption coefficient, σ_{ap}, yields the highest coefficient of determination, r^2, for January (0.7) and February (0.8) and lower values for December (0.4), March (0.4), and April (0.47). Lowest values (0.03 to 0.21) are obtained for May through November. Elevated levels of σ_{ap} at a wavelength of 550 nm indicate the presence of anthropogenic aerosol most likely in the form of soot from fossil fuel and biomass combustion. The regression results suggest that nss $SO_4^=$ and σ_{ap} are derived from the same source region during January and February but have different sources (perhaps in addition to a common source) during December, March, and April.

[35] Supermicron nss $SO_4^=$ concentrations are about an order of magnitude lower than submicron concentrations (Figure 4c and Table 3). There is a seasonal trend of highest mean concentrations in January and February, lower concentrations in March through June, and, with the exception of October, lowest concentrations in July through December.

[36] When using the $SO_4^=$ to Na^+ mass ratio for seawater of 0.252 to calculate supermicron nss $SO_4^=$ concentrations,

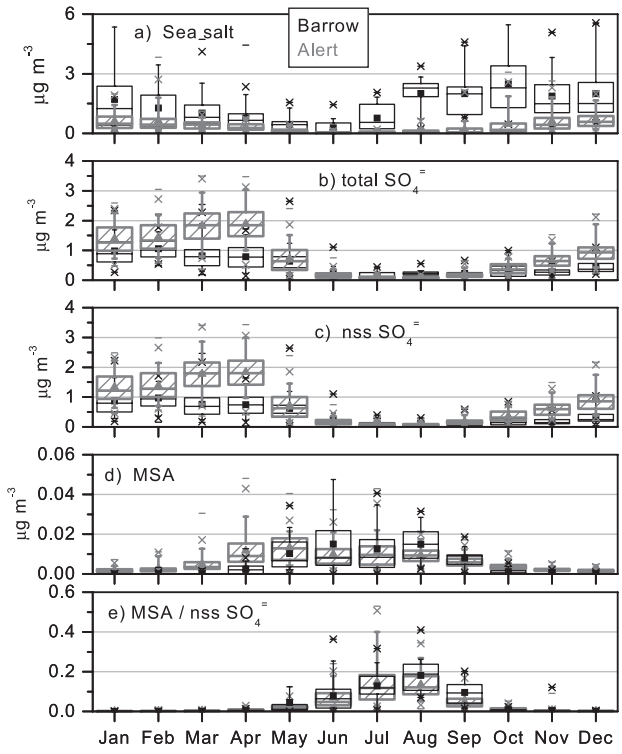

Figure 5. Box plots of total (submicron and supermicron) concentrations of (a) sea salt, (b) total $SO_4^=$, (c) nss $SO_4^=$, (d) MSA^-, and (e) MSA^- to nss $SO_4^=$ ratio from Barrow (black line) and Alert (hatched boxes) as a function of month. The Barrow data cover the period from October 1997 to December 2000, and the Alert data cover the period from July 1980 to May 1995. Percentile information is as in the Figure 1 caption.

31% of the samples have negative nss $SO_4^=$ concentrations. Negative nss $SO_4^=$ concentrations have also been reported for firn samples from near the Antarctic ice edge [*Gjessing*, 1984] and at several coastal Antarctic stations [*Wagenbach et al.*, 1988, 1998] and have been attributed to sea salt sulfate depletion. It has been hypothesized that sea salt sulfate depletion is driven by the crystallization of mirabilite ($Na_2SO_4 \cdot 10H_2O$) [*Richardson*, 1976; *Wagenbach et al.*, 1998]. Mirabilite is associated with the ice lattice. The remaining brine, which is not associated with the ice lattice, becomes depleted in $SO_4^=$ at temperatures below −8.2°C. It is not known, however, how the brine becomes preferentially airborne to form sea salt aerosol. With this process, sea salt particles directly emitted from ice-free seawater will not be fractionated.

[37] The negative nss $SO_4^=$ concentrations derived from using a seawater $SO_4^=$ to Na^+ ratio of 0.252 indicate that sea salt sulfate may also be depleted at Barrow in the supermicron size range. The degree of depletion is greatest for the winter and spring (see section 2). It is within experimental uncertainty for the summer season. The lack of a strong depletion in summer is consistent with the brine/sea ice hypothesis.

[38] Seasonal cycles of total measured $SO_4^=$ and nss $SO_4^=$ for the sum of the submicron and supermicron size ranges are similar at Barrow and Alert (Figures 5b and 5c). At both stations, total and nss $SO_4^=$ concentrations are lowest from June through September and increase steadily from October through February. In March and April, concentrations at Alert continue to increase, while they drop from the February values at Barrow. Mean concentrations are similar for May. The divergence of the seasonal cycles in March and April may be a result of different transport patterns of anthropogenic sulfate to Barrow and Alert and/or differences in the conversion processes of SO_2 to $SO_4^=$ either at or en route to the two stations. A long-term trend in sulfate may also be responsible in part since the Alert measurements cover the period of 1980 to 1995 and the Barrow measurements cover 1997 to 2000. *Sirois and Barrie* [1999] report a decrease in sulfate in the winter/spring months at Alert between 1991 and 1995. If this decrease is an Arctic-wide phenomenon that has persisted through 2000, it may account for some of the difference between the Alert and Barrow March/April sulfate concentrations. However, measurements of aerosol light scattering at Barrow give no indication of a decrease between 1991 and 1995. Scattering decreased between 1982 and 1992 [*Bodhaine and Dutton*, 1993] but has leveled off since then. In addition, sulfate measured during the three winter/spring seasons between 1997 and 2000 gives no indication of a decreasing trend at Barrow.

[39] Particulate NH_4^+ results from the reaction of gas phase NH_3 with acidic sulfate aerosol or other particulate anionic species. NH_3 has both natural and anthropogenic sources [*Prospero et al.*, 1996]. Natural sources include excreta from wild animals and emissions from soils, vegetation, and the ocean. Anthropogenic sources include fertilizer production and application, biomass burning, and excreta from domestic animals.

[40] The submicron NH_4^+ seasonal cycle at Barrow follows that of nss $SO_4^=$ with an increase in concentration in December and a broad peak from January through May (Figure 3d). Concentrations drop off sharply in June and remain at their lowest levels through November. The similarity in the behavior of NH_4^+ and nss $SO_4^=$ is most likely a result of the fast reaction of NH_3 with acidic sulfate aerosol near source regions outside of the Arctic. Mean monthly NH_4^+ to nss $SO_4^=$ molar ratios fall within a relatively narrow range of 1.5 to 1.75 for the winter and spring seasons indicating a molecular composition between ammonium bisulfate and ammonium sulfate. Mean ratios were lower (1.1 to 1.4) for the summer months indicating less availability of NH_4^+ to neutralize the sulfate aerosol. Supermicron NH_4^+ concentrations were more than an order of magnitude lower than the submicron concentrations (Table 3) and made up, on average, less than 1 ± 1.4% of the supermicron mass.

[41] Atmospheric methansulfonic acid or MSA^- is derived solely from the oxidation of biogenically produced DMS. The seasonal cycle of submicron MSA^- is out of phase relative to the other chemical species measured. Submicron concentrations begin to increase in April, peak in May through September, and drop sharply in October (Figure 3e and Table 2). Supermicron MSA^- shows the same seasonal behavior but only makes up 4 to 10% of the summed submicron and supermicron concentrations for those months in which it is detectable (May through October) (Table 3).

[42] The late spring elevated MSA^- concentrations may be a result of long-range transport from oceanic source regions in the North Pacific [*Li et al.*, 1993]. By late June, as the ice recedes in the Arctic and Bering Seas, phytoplankton productivity in surface waters begins, and DMS that is trapped under the ice is released. As the ice melt continues, the Arctic Ocean can become a substantial source of DMS through open leads and open ocean waters [*Ferek et al.*, 1995]. *Ferek et al.* [1995] measured atmospheric DMS concentrations at Barrow from May 31 to October 22, 1991, and found that concentrations were a few pptv in June, somewhat higher in July, and reached a maximum near 100 pptv in the middle of August before declining in early fall. In addition, *Levasseur et al.* [1994] suggested that DMS released by ice algae during the ice breakup may contribute to the early summer peak in DMS.

[43] Barrow and Alert seasonal cycles of MSA^- concentrations are compared in Figure 5d. They are similar in that both show a maximum in spring and summer. The cycles are slightly offset, however. Concentrations at Alert increase in March, peak in May, and show a second peak in July. The initial increase at Barrow starts a month later (April) followed by peaks in June and August. Monthly mean Barrow and Alert concentrations between May and September are within ±60%. MSA^- to nss $SO_4^=$ ratios have been used to determine the fraction of nss $SO_4^=$ that is biogenically produced [e.g., *Bates et al.*, 1992; *Li et al.*, 1993; *Huebert et al.*, 1996]. Monthly mean MSA^- to nss $SO_4^=$ ratios during the first MSA^- peak at Alert and Barrow are 0.02 ± 0.02 and 0.08 ± 0.09 (arithmetic means and 1σ standard deviation), respectively (Figure 5e). During the second peak, which occurs in the summer when anthropogenic nss $SO_4^=$ concentrations are expected to be lower, monthly mean ratios are 0.17 ± 0.19 and 0.18 ± 0.08 at Alert and Barrow, respectively.

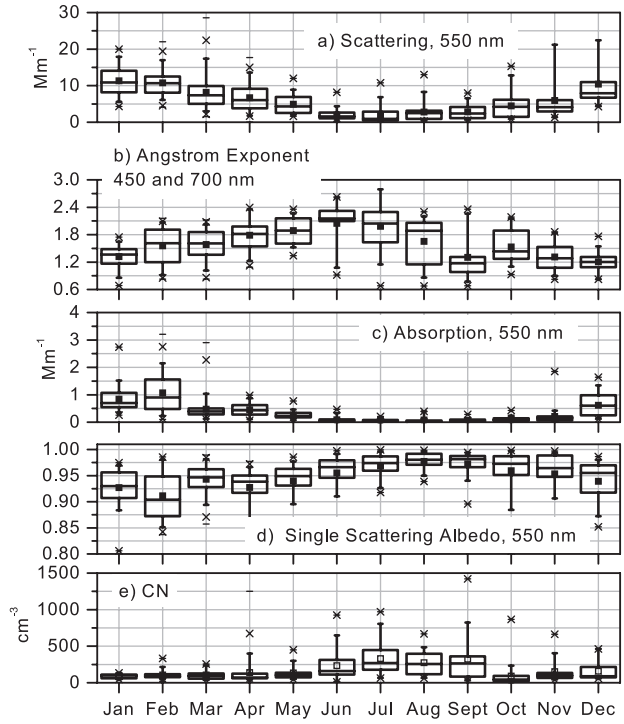

Figure 6. Box plots of submicron aerosol (a) scattering coefficient at 550 nm, (b) Ångström exponent for the 450 and 700 nm wavelength pair, (c) absorption coefficient at 550 nm, (d) single scattering albedo at 550 nm, and (e) the particle number concentration. Percentile information is as in the Figure 1 caption.

[44] The particle number concentration at Barrow shows a maximum in the summer months of June through September [*Polissar et al.*, 1999] (Figure 6e). During this time period the submicron aerosol light scattering coefficient is relatively low (Figure 6a), indicating that the increase in number concentration is due to small particles which are inefficient scatterers of light. It has been hypothesized that the summer maximum in particle concentration is related to the formation of biogenic sulfur particles [e.g., *Bodhaine*, 1989; *Polissar et al.*, 1999]. Measurements of vertical profiles of Aitken nucleus concentrations (diameters < 0.1 μm) and the light scattering coefficient west of Barrow during June of 1990 support this hypothesis [*Ferek et al.*, 1995]. Two flights during haze-free periods of moderate DMS concentration revealed high concentrations of Aitken nuclei between 0.5 and 2 km near the edges of stratus cloud layers from which snow was falling. Measurements of the light scattering coefficient showed no response to the high concentrations of Aitken nuclei, confirming the presence of small particles. *Ferek et al.* [1995] suggest that scavenging by the summertime low-level stratus clouds removes accumulation mode aerosol. The combination of low aerosol surface area and abundant biogenic aerosol precursor (DMS) leads to particle production thus influencing the particle number concentration aloft and at the surface.

[45] To further test the hypothesis, a linear regression of submicron MSA^- versus particle concentration was performed for the months with detectable MSA^- at Barrow. The resulting r^2 was 0.8 indicating a strong correlation between number concentration and biogenically derived aerosol mass.

[46] Non-sea-salt K^+ in submicron particles is a useful tracer of aerosol derived from biomass burning [e.g., *Andreae*, 1983; *Gaudichet et al.*, 1995]. Submicron nss K^+ concentrations at Barrow begin to increase in December, peak in January, and drop off from February through April (Figure 3f and Table 2). Lowest concentrations are observed in May to November. Hence nss K^+ follows the pattern of other species that are transported long distances during the winter/spring haze season. A linear regression of submicron nss K^+ versus nss $SO_4^=$ results in a poor correlation ($r^2 = 0.2$), however, confirming that they are derived from different sources; nss $SO_4^=$ is primarily a product of fossil fuel combustion and smelting of sulfide ores during this time of year [*Barrie et al.*, 1981], while nss K^+ results from biomass burning.

[47] Monthly mean supermicron nss K^+ concentrations range between 0.003 and 0.006 μg m^{-3}. They are of the same order of magnitude as summertime submicron concentrations but make up less than 0.3 ± 0.3% of the supermicron mass.

[48] Seasonal cycles of submicron nss Mg^{+2} and Ca^{+2} are shown in Figures 4g and 4h. Monthly mean concentrations of both ions are highest from December to March suggesting long-range transport from Eurasia. *Barrie and Barrie* [1990] attributed the presence of Mg and Ca in Alert aerosol to windblown soil. Soil dust from Asia has been observed in haze layers over Alaska [*Rahn et al.*, 1977] and the North Pacific [*Uematsu et al.*, 1985] during the springtime. Elevated aerosol Ca concentrations measured in the Norwegian Arctic during a March 1983 episode of long-range transport of pollutants from the former Soviet Union were attributed to metal emissions from coal combustion [*Pacyna and Ottar*, 1989]. Measurements of other trace elements found in soil dust (Al, Si, Ti, and Fe) would help to determine sources of the winter/spring maximum in nss Mg^{+2} and Ca^{+2} measured at Barrow. Low concentrations during the summer months indicate there is no strong local source of submicron nss Mg^{+2} and Ca^{+2} at Barrow.

[49] Supermicron nss Mg^{+2} concentrations peak in January through May and again in September through November (Figure 4d and Table 3). Supermicron nss Ca^{+2} concentrations exhibit a similar double-peaked annual cycle (Figure 4e and Table 3). This behavior suggests a distant source in the winter/spring months and a local source in the summer months. *Barrie and Barrie* [1990] reported a similar two-peaked annual cycle in soil dust (represented by Al) at Alert. Since the September soil dust peak does not coincide with elevated dust concentrations from northern hemisphere dust storms, they attributed it to the onset of snow on the ground and the resuspension of soil promoted by snow drifting over relatively bare soil.

5. Results: Seasonal Cycle of Optical Properties and Relationship to Chemical Compositions

[50] The magnitude of the scattering coefficient of a chemical component depends on its size-dependent mass (or volume) concentration. For a wavelength of 550 nm,

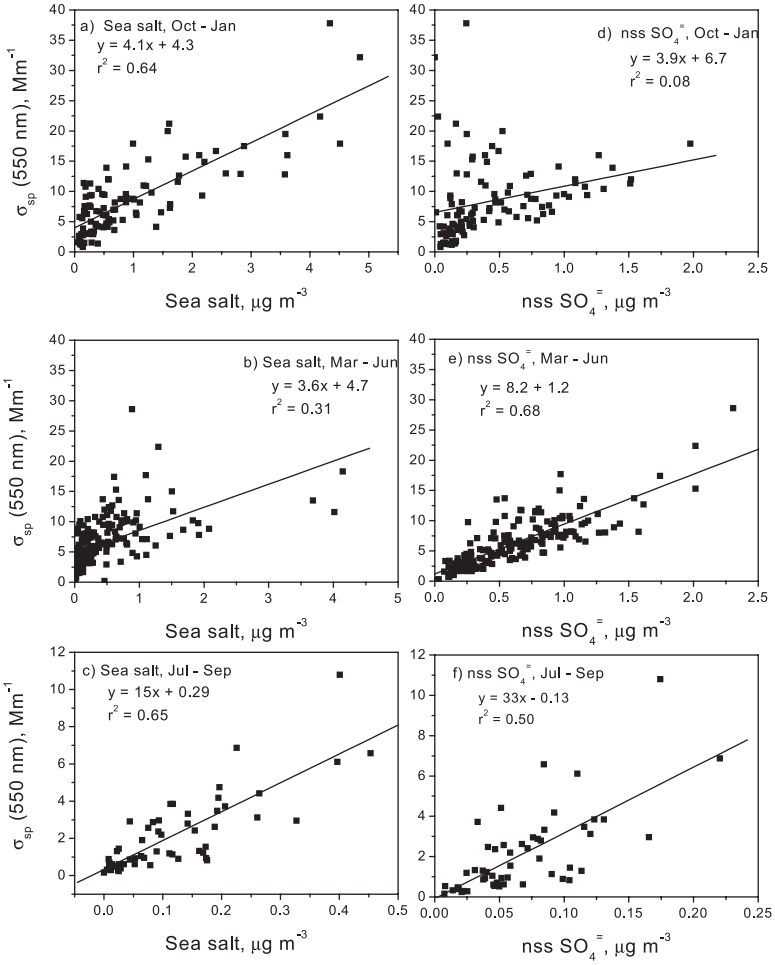

Figure 7. Linear regression of the mass concentrations of submicron sea salt or nss $SO_4^=$ versus submicron σ_{sp}(550 nm) for the winter, spring, and summer seasons. Sea salt versus σ_{sp}(550 nm) is shown for (a) October to January, (b) March to June, and (c) July to September. Non-sea-salt $SO_4^=$ versus σ_{sp}(550 nm) is shown for (d) October to January, (e) March to June, and (f) July to September.

particles of unit volume, and a refractive index of $1.5-10^{-7}$i, which is near that of $(NH_4)_2SO_4$ and sea salt at low RH, the scattering efficiency is lognormally distributed with the most efficient size range for scattering occurring between particle diameters of 0.2 and 1.0 μm [*Quinn et al.*, 1996]. In addition, it is the submicron particles that are transported over long distances as deposition rates increase with particle size. Therefore the discussion of aerosol optical properties measured at Barrow focuses on the submicron size range.

[51] The seasonal cycle of σ_{sp} at Barrow has been described previously by *Bodhaine* [1989] (for measurements from 1976 to 1986) and *Bodhaine and Dutton* [1993] (for measurements from 1976 to 1993). These measurements were made on non-size- segregated aerosol and therefore did not consider the submicron and supermicron size ranges separately. This long-term record shows maximum values of σ_{sp} in March and April that drop off in May and reach the lowest values of the year in June. *Bodhaine* [1989] also comment on episodic events of high σ_{sp} and low Ångström exponents (indicating a relatively large-sized aerosol) in October and November and hypothesize that these could be caused by sea salt or windblown dust.

[52] The seasonal cycle in submicron σ_{sp} measured since October of 1997 (when the aerosol sampling system was changed at Barrow to include a high-sensitivity nephelometer sampling size-segregated aerosol at a reference RH) is similar to that reported by *Bodhaine* [1989] and *Bodhaine and Dutton* [1993] for the bulk aerosol. Scattering by submicron aerosol begins to increase in October, is highest in December through April, decreases in May, and drops to lowest levels in June through September (Figure 6a). This trend follows the combined trends of submicron sea salt and nss $SO_4^=$, the two dominant ionic aerosol chemical components at Barrow. A linear regression of σ_{sp}(550nm) against sea salt mass concentrations for the months of October through January, the period of high sea salt and relatively low nss $SO_4^=$ concentrations, results in a coefficient of determination, r^2, of 0.64 (Figure 7a). On the basis of this analysis, sea salt can explain about 60% of the variance in scattering for the submicron size range for this period of the year. The October through January regression for σ_{sp}(550 nm) versus nss $SO_4^=$ results in r^2 of 0.08 (Figure 7d). The correlation between measured σ_{sp} and sea salt concentrations confirms the hypothesis of *Bodhaine* [1989] that sea salt influences light scattering during October and November.

Table 4. Submicron Mass Scattering Efficiencies for the Dominant Aerosol Components (nss $SO_4^=$ and Sea Salt), the Residual Mass, and the Total Submicron Aerosol[a]

Season	Number of Samples	$\alpha_{sp,SO4,ion}$, $m^2\ g^{-1}$	$\alpha_{sp,seasalt}$, $m^2\ g^{-1}$	$\alpha_{sp,res}$, $m^2\ g^{-1}$	$\alpha_{sp,sub,aer}$, $m^2\ g^{-1}$
Oct.–Jan.	69	5.8 ± 1.0	1.8 ± 0.37	1.3 ± 0.63	2.4 ± 0.15
March–June	124	5.6 ± 0.32	2.9 ± 0.26	0.21 ± 0.31	2.9 ± 0.20
July–Sept.	40	4.1 ± 2.9	5.1 ± 0.97	1.5 ± 1.0	3.7 ± 0.49
All year	289	5.3 ± 0.28	2.2 ± 0.15	0.82 ± 0.26	2.5 ± 0.09

[a] Values are reported at 33% RH and given as average plus or minus standard error.

[53] Concentrations of submicron nss $SO_4^=$ are comparable to those of submicron sea salt in March and higher than those of sea salt in April, May, and June. A linear regression of submicron $\sigma_{sp}(550)$ versus nss $SO_4^=$ for March through June results in an r^2 equal to 0.68 indicating that nss $SO_4^=$ can explain about 70% of the variance during the spring (Figure 7c). The March through June regression for sea salt yields an $r^2 = 0.31$ (Figure 7b).

[54] Submicron mass concentrations are lowest in July through September. During this summer period both sea salt and nss $SO_4^=$ appear to contribute to $\sigma_{sp}(550\ nm)$. The value of r^2 for $\sigma_{sp}(550\ nm)$ versus sea salt is 0.65 (Figure 7c) and for nss $SO_4^=$ is 0.50 (Figure 7f).

[55] On the basis of these results, for the submicron size range, sea salt has a dominant role in controlling $\sigma_{sp}(550$ nm) in the winter, nss $SO_4^=$ is dominant in the spring, and both components contribute to $\sigma_{sp}(550\ nm)$ in the summer.

[56] The Ångström exponent, å, for the 450 and 700 nm nephelometer wavelength pair was calculated from

$$\text{å} = -\frac{\log\left(\sigma_{sp}(450)/\sigma_{sp}(700)\right)}{\log\left(450/700\right)}. \quad (2)$$

Similar to what was reported by *Bodhaine* [1989], there is an increase in å from January to June (Figure 6b) indicating a shift in the aerosol population to relatively smaller particles. *Bodhaine* [1989] attributed this increase to more efficient gas-to-particle conversion during transport from lower latitudes as the solar elevation increases. Values remain high for the months of June through August which corresponds to the time of year of lowest aerosol mass concentrations and scattering coefficients and highest MSA^- and particle number concentrations. The simultaneous occurrence of relatively small diameter particles and high MSA^- and particle number concentrations further confirms that these particles are a result of local biogenic origin.

[57] The lower values of å during the months of October to January indicate a population of relatively larger submicron particles. On the basis of the chemical analysis these larger diameter particles are most likely due to the influx of sea salt to Barrow from the northern Pacific Ocean.

[58] In general, the seasonal cycle of the submicron absorption coefficient, $\sigma_{ap}(550)$, follows that of the scattering coefficient (Figure 6c). (A linear regression of the monthly arithmetic mean scattering versus absorption coefficient yields an r^2 of 0.88.) There are differences between the two seasonal cycles, however, that affect the seasonal cycle of single scattering albedo. The mean absorption coefficient peaks in February, while $\sigma_{sp}(550$ nm) peaks in January to February. In addition, the annual cycle of $\sigma_{ap}(550$ nm) is stronger than $\sigma_{sp}(550$ nm). This difference most likely is a result of the low frequency of long-range transport of anthropogenic absorbing aerosol to the site in summer along with a summertime source of biogenic scattering aerosol. Hence the absorption coefficient appears to be the less ambiguous marker for imported pollution.

[59] Monthly percentile information for the aerosol single scattering albedo, defined as

$$\omega = \sigma_{sp}/\left(\sigma_{sp} + \sigma_{ap}\right), \quad (3)$$

is shown in Figure 6d. Values of ω are lowest in the winter and spring (December through April) with a minimum value in February (0.91 ± 0.04, arithmetic mean and 1σ standard deviation) corresponding to the peak in σ_{ap}. Values begin to

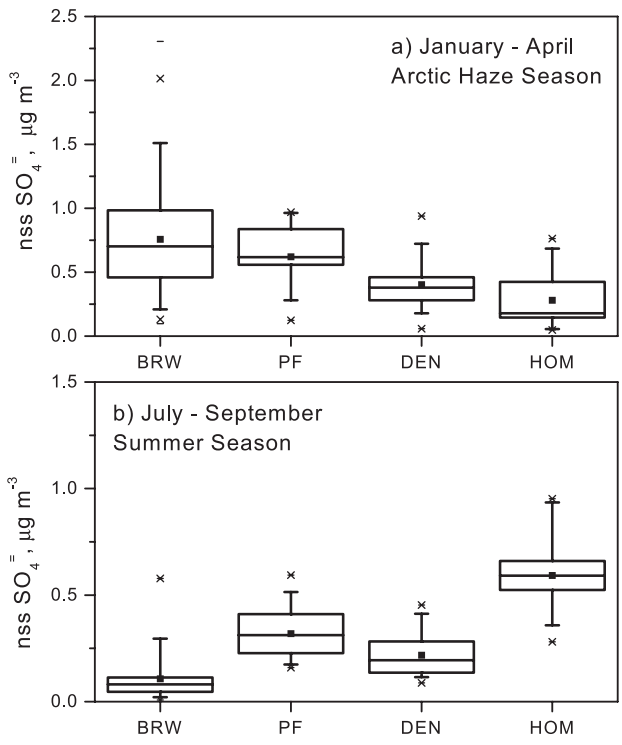

Figure 8. Comparison of nss $SO_4^=$ concentrations from October 1997 to December 1999 measured at Barrow (BRW), Poker Flat Rocket Range (PF), Denali National Park (DEN), and Homer (HOM). Shown are data from the (a) winter/spring haze season (January to April) and (b) summer (July to September). Percentile information is as in the Figure 1 caption.

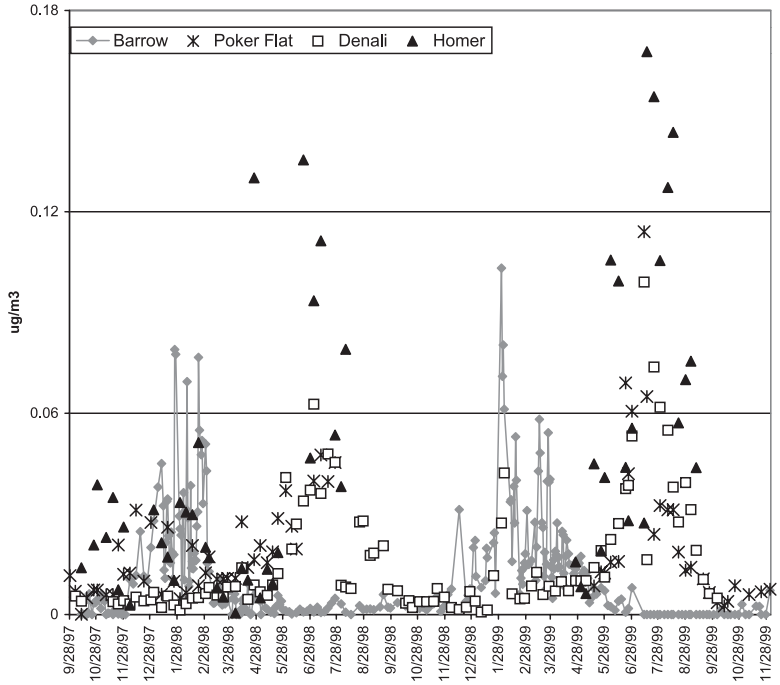

Figure 9. Non-sea-salt K^+ for October 1997 to December 1999 at Barrow, Poker Flat, Denali National Park, and Homer.

increase in May, reach a maximum in August (0.98 ± 0.02), and then steadily decrease through December. The summer maximum results from the lack of a source of summertime absorbing aerosol.

[60] The mass scattering efficiency of a chemical component links the mass concentration of that component to its light scattering efficiency. It is an essential quantity for calculating its direct climate forcing [*Charlson et al.*, 1999]. Mass scattering efficiencies for individual aerosol chemical components can be estimated from a multiple linear regression of the mass concentration of each aerosol component against the scattering coefficient for the whole aerosol. An equation of the following form, including only the major aerosol components, was used to obtain weighted averages of the submicron mass scattering efficiencies:

$$\alpha_{sp} = \alpha_{sp,seasalt} m_{seasalt} + \alpha_{sp,SO4,ion} m_{SO4,ion} + \alpha_{sp,res} m_{res}, \quad (4)$$

where σ_{sp} is the measured submicron value, $\alpha_{sp,j}$ is the submicron mass scattering efficiency of component j, and m_j is the submicron mass concentration of component j which, for sea salt and sulfate, includes associated water at the measurement RH. In addition, the mass scattering efficiency of the total submicron aerosol, $\alpha_{sp,sub,aer}$ was calculated from a linear regression of the submicron mass concentration versus the submicron measured σ_{sp}. Calculations were done for the entire year, winter (October to January), spring (March to June), and summer (July to September). Resulting mass scattering efficiencies are reported in Table 4.

[61] Average values of $\alpha_{sp,SO4,ion}$ were relatively constant over all seasons with weighted averages ranging from 4.1 ± 2.9 to 5.8 ± 1.0 $m^2\ g^{-1}$. The consistency of the values most likely is a result of the stability in the nss $SO_4^=$ size distribution over the course of a year. Values of $\alpha_{sp,seasalt}$ and $\alpha_{sp,res}$ vary more with season indicating a more variable size distribution. The relatively large values of $\alpha_{sp,seasalt}$ for the months of July through September suggest that more coarse mode sea salt mass extends in the optically efficient size range (0.2 to 1.0 μm) during this time of year. This is consistent with a local source of sea salt such that the aerosol is not transported over long distances with a loss of large particle mass through deposition processes. The mass scattering efficiencies for nss $SO_4^=$ ion and sea salt calculated for the Barrow aerosol fall within the range of those determined for the central Pacific Ocean atmosphere [*Quinn et al.*, 1996]. In addition, the Barrow $\alpha_{sp,SO4,ion}$ fall within the theoretical range of low RH sulfate scattering efficiencies predicted by *Charlson et al.* [1999].

6. Results: Comparison of Aerosol Chemical Composition From Four Alaskan Sites

[62] Three sites in addition to Barrow form the Alaskan aerosol sampling network. These are located, from north to south, at Poker Flat Rocket Range (65.1°N, 147.5°W), Denali National Park (63.45°N, 149.3°W), and Homer (59.7°N, 151.5°W). Using high-volume, non-size-segregated samplers, weekly samples have been collected at Poker Flat and Homer since 1995 and at Denali since 1997. The data from these sites are compared to those from Barrow to determine how far south Arctic Haze extended during the 1997/1998 and 1998/1999 haze seasons.

[63] Data were divided into the haze season (January to April) when nss $SO_4^=$ concentrations are highest and anthropogenic influences are greatest and the summer season (July to September) when nss $SO_4^=$ concentrations are lowest. Percentile information for nss $SO_4^=$ concentra-

tions for the four sites are shown in Figure 8. During the haze season, concentrations are highest at Barrow and decrease with latitude from Poker Flat to Denali to Homer. The Brooks Range runs east-west south of Barrow and is north of all of the other sites. It serves as a barrier to transport of aerosol to southern latitudes and is one explanation for why winter/spring concentrations of nss $SO_4^=$ are highest at Barrow. A second mountain range, the Alaska Range, runs east-west north of Homer further isolating this southernmost site from the impact of Arctic Haze. As a result, concentrations of nss $SO_4^=$ are the lowest here of the four sites during the haze season. *Polissar et al.* [1998], assuming all measured elemental sulfur was due to $SO_4^=$, reported a similar gradient in maximum nss $SO_4^=$ concentration from northwest to southeast Alaska during the winter and spring months.

[64] In July through September, concentrations of nss $SO_4^=$ are lowest at Barrow and highest at Homer. The source of the summertime nss $SO_4^=$ at Homer may be biogenic from DMS emissions in the Gulf of Alaska and Cooke Inlet. Past and future samples collected at Homer will be analyzed for MSA^- to test this hypothesis.

[65] Also compared were seasonal cycles of nss K^+ at the four sites (Figure 9). As described in section 4.2, nss K^+ concentrations at Barrow peak in December through April and are at a minimum in May through November following the trend of other chemical species that make up the winter/spring Arctic Haze. In contrast, nss K^+ concentrations at Poker Flat, Denali, and Homer peak in the summer months most likely due to local and/or regional forest fires. *Polissar et al.* [1996] found a correlation between summer peaks of aerosol optical absorption and fire activity for Gates of the Arctic National Park and Denali during 1988, 1990, and 1991 and concluded that wood smoke from forest fires is one of the most important regional sources of aerosol during summer. On average, during the period from 1960 to 1997, 280,000 ha of boreal forest burned in Alaska each summer with the peak in the fire season occurring in July and August [*Lavoue et al.*, 2000].

7. Conclusions

[66] Presented here are results from the longest reported record of simultaneously measured aerosol chemical and optical properties at Barrow, Alaska. Measurements have been made since October of 1997 to present. Such simultaneous measurements allow for the identification of the chemical components responsible for observed changes in aerosol optical properties on seasonal, annual, and longer timescales. Continuous measurements of aerosol ionic chemical composition and light scattering indicate that sea salt is dominant in controlling light scattering during winter, nss $SO_4^=$ dominates in spring, and both play a role in summer. In addition, the mass fraction of residual (chemically unanalyzed) mass is equal to the ionic mass fraction for the submicron size range in summer suggesting a role for unidentified organic species in controlling aerosol light scattering.

[67] A strong correlation between MSA^- and particle number concentration during the summer indicates a source of biogenic particles during this time of year. Low submicron aerosol scattering coefficients and high Ångström exponents indicate the presence of smaller diameter submicron particles providing further evidence for this hypothesis. It is likely that at least a portion of the summertime residual mass also is of biogenic origin as there are no strong anthropogenic sources of aerosol during this time of year.

[68] Mass scattering efficiencies of submicron nss $SO_4^=$ are relatively constant with season indicating a stable size distribution throughout the year. Values for submicron sea salt are more variable with season most likely due to varying amounts of coarse mode sea salt tailing into the submicron size range. Higher values occur during the summer when supermicron sea salt concentrations are at a maximum.

[69] Non-sea-salt $SO_4^=$ concentrations during the haze season (January through April) decrease with decreasing latitude from Barrow south to Homer. Hence there appears to be a latitudinal gradient in the extent of Arctic haze. In contrast, nss $SO_4^=$ concentrations at Homer are highest during the summer presumably due to a stronger biogenic source. This needs to be confirmed with measurements of MSA^- concentrations, however.

[70] The 3-year record of aerosol measurements presented here has allowed for the assessment of seasonal changes in aerosol optical properties with respect to changes in aerosol ionic composition. A longer data record is needed, however, to determine longer-term trends in Arctic Haze and to detect changes in aerosol sources and transport pathways to the Arctic associated with climate change. In addition, other questions remain including what the substantial submicron residual mass during the summer is composed of. With more complete chemical analysis, including routine measurements of organic carbon, black carbon, and trace elements, it would be possible to address this question and that of changing aerosol sources and transport to the Arctic.

[71] **Acknowledgments.** We thank Dan Endres and Andrea Blakesley for help in collecting samples at Barrow, Denali, Poker Flat, and Homer. We thank Derek Coffman for performing the thermodyamic equilibrium model calculations, Jim Johnson for the trajectory calculations, and Drew Hamilton for logistical assistance. The Alert data were graciously provided by Len Barrie and the Meteorological Service of Canada. This work was supported by NOAA's Arctic Program and NOAA's Office of Global Programs' Aerosol Program. This is PMEL contribution 2367 and JISAO contribution 853.

References

Anderson, T. L., and J. A. Ogren, Determining aerosol radiative properties using the TSI 3563 integrating nephelometer, *Aerosol Sci. Technol.*, *29*, 57–69, 1998.

Andreae, M. O., Soot carbon and excess fine potassium: Long-range transport of combustion-derived aerosols, *Science*, *220*, 1148–1151, 1983.

Ayers, G. P., M. D. Keywood, and J. L. Gras, TEOM vs. manual gravimetric methods for determination of PM2.5 aerosol mass concentrations, *Atmos. Environ.*, *33*, 3717–3721, 1999.

Barrie, L. A., and M. J. Barrie, Chemical components of lower tropospheric aerosols in the high Arctic: Six years of observations, *J. Atmos. Chem.*, *11*, 211–226, 1990.

Barrie, L. A., and R. M. Hoff, The oxidation rate and residence time of sulphur dioxide in the Arctic atmosphere, *Atmos. Environ.*, *18*, 2711–2722, 1984.

Barrie, L. A., R. M. Hoff, and S. M. Daggupaty, The influence of mid-latitudinal pollution sources on haze in the Canadian Arctic, *Atmos. Environ.*, *15*, 1407–1419, 1981.

Barrie, L. A., M. P. Olson, and K. K. Oikawa, The flux of anthropogenic sulphur into the Arctic from mid-latitudes in 1979/80, *Atmos. Environ.*, *23*, 2505–2512, 1989.

Bates, T. S., J. A. Calhoun, and P. K. Quinn, Variations in the concentration ratio of methane-sulfonate to sulfate in marine aerosol particles over the South Pacific Ocean, *J. Geophys. Res.*, *97*, 9859–9865, 1992.

Berner, A., C. Lurzer, F. Pohl, O. Preining, and P. Wagner, The size distribution of the urban aerosol in Vienna, *Sci. Total Environ.*, *13*, 245–261, 1979.

Bodhaine, B. A., Barrow surface aerosol: 1976–1986, *Atmos. Environ.*, *23*, 2357–2369, 1989.

Bodhaine, B. A., Aerosol absorption measurements at Barrow, Mauna Loa, and the South Pole, *J. Geophys. Res.*, *100*, 8967–8975, 1995.

Bodhaine, B. A., and E. G. Dutton, A long-term decrease in Arctic haze at Barrow, Alaska, *Geophys. Res. Lett.*, *20*, 947–950, 1993.

Bond, T. C., T. L. Anderson, and D. Campbell, Calibration and intercomparison of filter-based measurements of visible light absorption by aerosols, *Aerosol Sci. Technol.*, *30*, 582–600, 1999.

Bridgman, H. A., and B. A. Bodhaine, On the frequency of long-range transport events at Point Barrow, Alaska, 1983–1992, *Atmos. Environ.*, *28*, 3537–3549, 1994.

Charlson, R. J., T. L. Anderson, and H. Rodhe, Direct climate forcing by anthropogenic aerosols: Quantifying the link between atmospheric sulfate and radiation, *Contrib. Atmos. Phys.*, *72*(1), 79–94, 1999.

Delene, D. J., and J. A. Ogren, Variability of aerosol optical properties at four North American surface monitoring sites, *J. Atmos. Sci.*, *59*(6), 1135–1150, 2002.

Draxler, R. R., Hybrid Single-Particle Lagrangian Integrated Trajectories (HY-SPLIT): Version 3.0. user's guide and model description, *Tech. Rep. ERL ARL-195*, Natl. Oceanic and Atmos. Admin., Silver Spring, Md., 1992.

Ferek, R. J., P. V. Hobbs, L. F. Radke, J. A. Herring, W. T. Sturges, and G. F. Cota, Dimethyl sulfide in the arctic atmosphere, *J. Geophys. Res.*, *100*, 26,093–26,104, 1995.

Gaudichet, A., F. Echalar, B. Chatenet, J. P. Quisefit, G. Malingre, H. Cachier, P. Buat-Menard, P. Artaxo, and W. Maenhaut, Trace elements in tropical African savanna biomass burning aerosols, *J. Atmos. Chem.*, *22*, 19–39, 1995.

Gjessing, Y., Marine and non-marine contribution to the chemical composition of snow at the Riiser-Larsen ice shelf in Antarctica, *Atmos. Environ.*, *23*, 155–160, 1984.

Heintzenberg, J., and S. Larssen, SO_2 and SO_4 in the Arctic: Interpretation of observations at three Norwegian Arctic-Subarctic stations, *Tellus, Ser. B*, *35*, 255–265, 1983.

Holland, H. D., *The Chemistry of the Atmosphere and Oceans*, p. 154, John Wiley, New York, 1978.

Hopper, J. F., D. E. J. Worthy, L. A. Barrie, and N. B. A. Trivett, Atmospheric observations of aerosol black carbon, carbon dioxide, and methane in the high Arctic, *Atmos. Environ.*, *28*, 3047–3054, 1994.

Huebert, B. J., D. J. Wylie, and J. A. Heath, Production and loss of methanesulfonate and non-sea-salt sulfate in the equatorial Pacific marine boundary layer, *Geophys. Res. Lett.*, *23*, 737–740, 1996.

Iversen, T., and E. Joranger, Arctic air pollution and large-scale atmospheric flows, *Atmos. Environ.*, *19*, 2099–2108, 1985.

Langner, J., and H. Rodhe, A global three-dimensional model of the tropospheric sulfur cycle, *J. Atmos. Chem.*, *13*, 225–263, 1991.

Lavoue, D., C. Liousse, H. Cachier, B. J. Stocks, and J. G. Goldhammer, Modeling of carbonaceous particles emitted by boreal and temperate wild fires at northern latitudes, *J. Geophys. Res.*, *105*, 26,871–26,890, 2000.

Levasseur, M., M. Gosselin, and S. Michaud, A new source of dimethylsulfide (DMS) for the arctic atmosphere: Ice diatoms, *Mar. Biol.*, *121*, 381–387, 1994.

Li, S. M., and J. W. Winchester, Geochemistry of organic and inorganic ions of late winter Arctic aerosols, *Atmos. Environ.*, *23*, 2401–2415, 1989.

Li, S. M., L. A. Barrie, and A. Sirois, Biogenic sulfate aerosol in the Arctic troposphere, 2, Trends and seasonal variations, *J. Geophys. Res.*, *98*, 20,623–20,631, 1993.

Lowenthal, D. H., and K. A. Rahn, Regional sources of pollution aerosol at Barrow, Alaska, during winter 1979–80 as deduced from elemental tracers, *Atmos. Environ.*, *19*, 2011–2024, 1985.

Meyer, M., J. Lijek, and D. Ono, Continuous PM10 measurements in a woodsmoke environment, in *PM10 Standards and Nontraditional Particulate Source Controls*, edited by J. C. Chow and D. M. Ono, vol. 1, *Tech. Rep. TR-22*, pp. 2–38, Air and Waste Manage. Assoc., Pittsburgh, Pa., 1992.

Norman, A. L., L. A. Barrie, D. Toom-Sauntry, A. Sirois, H. R. Krouse, S. M. Li, and S. Sharma, Sources of aerosol sulfate at Alert: Apportionment using stable isotopes, *J. Geophys., Res.*, *104*, 11,619–11,631, 1999.

Pacyna, J. M., and B. Ottar, Origin of natural constituents in the Arctic aerosol, *Atmos. Environ.*, *23*, 809–811, 1989.

Polissar, A. V., P. K. Hopke, W. C. Malm, and J. F. Sisler, The ratio of aerosol optical absorption coefficients to sulfur concentrations as an indicator of smoke from forest fires when sampling in polar regions, *Atmos. Environ.*, *30*, 1147–1157, 1996.

Polissar, A. V., P. K. Hopke, W. C. Malm, and J. F. Sisler, Atmospheric aerosol over Alaska, 1, Spatial and seasonal variability, *J. Geophys. Res.*, *103*, 19,035–19,044, 1998.

Polissar, A. V., P. K. Hopke, P. Paatero, Y. J. Kaufmann, D. K. Hall, B. A. Bodhaine, E. G. Dutton, and J. M. Harris, The aerosol at Barrow, Alaska: Long-term trends and source locations, *Atmos. Environ.*, *33*, 2441–2458, 1999.

Prospero, J. M., K. Barrett, T. Church, F. Dentener, R. A. Duce, J. N. Galloway, H. Levy, J. Moody, and P. Quinn, Atmospheric deposition of nutrients to the North Atlantic Basin, *Biogeochemistry*, *35*, 27–73, 1996.

Quinn, P. K., and D. J. Coffman, Local closure during ACE 1: Aerosol mass concentration and scattering and backscattering coefficients, *J. Geophys. Res.*, *103*, 16,575–16,596, 1998.

Quinn, P. K., V. N. Kapustin, T. S. Bates, and D. S. Covert, Chemical and optical properties of marine boundary layer aerosol particles of the mid-Pacific in relation to sources and meteorological transport, *J. Geophys. Res.*, *101*, 6931–6951, 1996.

Quinn, P. K., D. J. Coffman, V. N. Kapustin, T. S. Bates, and D. S. Covert, Aerosol optical properties in the marine boundary layer during ACE 1 and the underlying chemical and physical aerosol properties, *J. Geophys. Res.*, *103*, 16,547–16,563, 1998.

Quinn, P. K., et al., Surface submicron aerosol chemical composition: What fraction is not sulfate?, *J. Geophys. Res.*, *105*, 6785–6806, 2000.

Rahn, K. A., The Mn/V ratio as an indicator of large-scale sources of pollution aerosol for the Arctic, *Atmos. Environ.*, *15*, 1457–1464, 1981a.

Rahn, K. A., Relative importances of North America and Eurasia as sources of Arctic aerosol, *Atmos. Environ.*, *15*, 1447–1455, 1981b.

Rahn, K. A., R. D. Borys, and G. E. Shaw, The Asian source of Arctic haze bands, *Nature*, *268*, 713–715, 1977.

Richardson, C., Phase relationship in sea ice as function of temperatures, *J. Glaciol.*, *17*, 507–519, 1976.

Schnell, R. C., T. B. Watson, and B. A. Bodhaine, NOAA WP-3D instrumentation and flight operations on AGASP-II, *J. Atmos. Chem.*, *9*, 3–16, 1989.

Shaw, G. E., Eddy diffusion transport of Arctic pollution from the mid-latitudes: A preliminary model, *Atmos. Environ.*, *15*, 1483–1490, 1981.

Sirois, A., and L. A. Barrie, Arctic lower tropospheric aerosol trends and composition at Alert, Canada: 1980–1995, *J. Geophys. Res.*, *104*, 11,599–11,618, 1999.

Sturges, W. T., and L. A. Barrie, Chlorine, bromine, and iodine in Arctic aerosols, *Atmos. Environ.*, *22*, 1179–1194, 1988.

Uematsu, M., R. A. Duce, and J. M. Prospero, Deposition of atmospheric mineral particles in the North Pacific Ocean, *J. Atmos. Chem.*, *3*, 123–128, 1985.

Wagenbach, D., U. Gorlach, and K. Moser, Coastal Antarctic aerosol: The seasonal pattern of its chemical composition and radionuclide content, *Tellus*, *40*, 426–436, 1988.

Wagenbach, D., F. Ducroz, R. Mulvaney, L. Keck, A. Minikin, J. Legrand, J. S. Hall, and E.W. Wolff, Sea-salt aerosol in coastal Antarctic regions, *J. Geophys. Res.*, *103*, 10,961–10,974, 1998.

Watts, S. F., R. Yaaqub, T. Davies, D. H. Lowenthal, K. A. Rahn, R. M. Harrison, B. T. Storr, and J. L. Baker, The use of Whatman 41 filter papers for high-volume aerosol sampling, *Atmos. Environ.*, *21*, 2731–2736, 1987.

E. Andrews and J. A. Ogren, Climate Monitoring and Diagnostics Laboratory, NOAA, 325 Broadway R/CMDL, Boulder, CO 80305, USA.

T. S. Bates, T. L. Miller, and P. K. Quinn, Pacific Marine Environmental Laboratory, NOAA, 7600 Sand Point Way NE, Seattle, WA 98115-6349, USA. (quinn@pmel.noaa.gov)

G. E. Shaw, Geophysical Institute, University of Alaska, Fairbanks, AK 99775, USA.